BIOPHOTONICS

A tunable reflector enabling crustaceans to see but not be seen

Keshet Shavit[1], Avital Wagner[1], Lukas Schertel[2,3], Viviana Farstey[4], Derya Akkaynak[4,5], Gan Zhang[1]†, Alexander Upcher[6], Amir Sagi[7,8], Venkata Jayasurya Yallapragada[9], Johannes Haataja[2]*, Benjamin A. Palmer[1]*

Many oceanic prey animals use transparent bodies to avoid detection. However, conspicuous eye pigments, required for vision, compromise the organisms' ability to remain unseen. We report the discovery of a reflector overlying the eye pigments in larval decapod crustaceans and show how it is tuned to render the organisms inconspicuous against the background. The ultracompact reflector is constructed from a photonic glass of crystalline isoxanthopterin nanospheres. The nanospheres' size and ordering are modulated to tune the reflectance from deep blue to yellow, enabling concealment in different habitats. The reflector may also function to enhance the acuity or sensitivity of the minute eyes by acting as an optical screen between photoreceptors. This multifunctional reflector offers inspiration for constructing tunable artificial photonic materials from biocompatible organic molecules.

Many pelagic animals (such as jellyfish, mollusks, and fish) use transparent bodies to appear invisible in the ocean as a defense against predation (*1*). However, to enable vision, these organisms require highly conspicuous eye pigments that enhance their risk of being detected (*2*, *3*). Transparent organisms have developed ingenious strategies to circumvent this trade-off between seeing and not being seen (*4*), including reducing the size and visibility of eyes (*5*) and retinas (*6*) or using mirrored irises (*7*) to conceal eye pigments. In addition to possessing condensed retinas (*6*), larval crustaceans use an alternative strategy: a reflector overlying the opaque eye pigments whose color is matched to the background, providing crypsis (*2*, *3*). This reflector produces a characteristic eyeshine distinct from the reflectance of tapeta lucida displayed by many other organisms. The eyeshine phenomenon is present in many larval *Malacostracans* (*8*–*11*), but the nature of the photonic structure is unknown.

We show that the eyeshine of larval decapods is produced by a photonic glass [a disordered assembly of wavelength-sized, dielectric spheres that express resonant scattering behavior (*12*–*14*)], constructed from high refractive index nanospheres (*15*, *16*). Deep blue to yellow-green eyeshine in different species is produced by tuning the size of the crystalline nanospheres, enabling crypsis in aquatic habitats with different optical properties. We observed that some decapod species also change their eyeshine color when subjected to different light intensities (dark and light adaptation). This is achieved through a modulation in nanosphere ordering and suggests an ability to dynamically match their eyeshine to a changing background. The reflector may also function to screen cross-talk between adjacent photoreceptors, potentially mitigating against the visual costs of having extremely small eyes.

To investigate the eyeshine phenomenon, we studied a model species of freshwater prawn, *Macrobrachium rosenbergii* (Fig. 1A), as well as larval crustaceans collected from the Gulf of Aqaba (Fig. 1, B to I, and supplementary materials). The collected prawn, shrimp, lobster, stomatopod, and crab larvae have completely transparent bodies but exhibit striking blue, green, silver, and yellow-green eyeshine (Fig. 1).

Ultrastructural properties of the reflector

To determine the structural origin of the eyeshine, the brilliant yellow-green eyes of *M. rosenbergii* were imaged by means of optical (Fig. 2, A to C) and cryogenic scanning electron microscopy

[1]Department of Chemistry, Ben-Gurion University of the Negev, Beer-Sheva 8410501, Israel. [2]Yusuf Hamied Department of Chemistry, University of Cambridge, Cambridge CB2 1EW, U.K. [3]Department of Physics, University of Fribourg, 1700 Fribourg, Switzerland. [4]The Interuniversity Institute for Marine Sciences, Eilat 8810302, Israel. [5]Hatter Department of Marine Technologies, University of Haifa, Haifa 3498838, Israel. [6]Ilse Katz Institute for Nanoscale Science & Technology, Ben-Gurion University of the Negev, Be'er Sheba 8410501, Israel [7]Department of Life Sciences, Ben-Gurion University of the Negev, Beer-Sheva 8410501, Israel. [8]The National Institute for Biotechnology in the Negev, Ben-Gurion University of the Negev, Beer-Sheva 8410501, Israel. [9]Department of Physics, Indian Institute of Technology Kanpur, Kanpur, Uttar Pradesh 208016, India.
***Corresponding author. Email: jh2225@cam.ac.uk (J.H.); bpalmer@bgu.ac.il (B.A.P.)**
†Present address: College of Chemistry and Chemical Engineering, Lanzhou University, Lanzhou 730000, China.

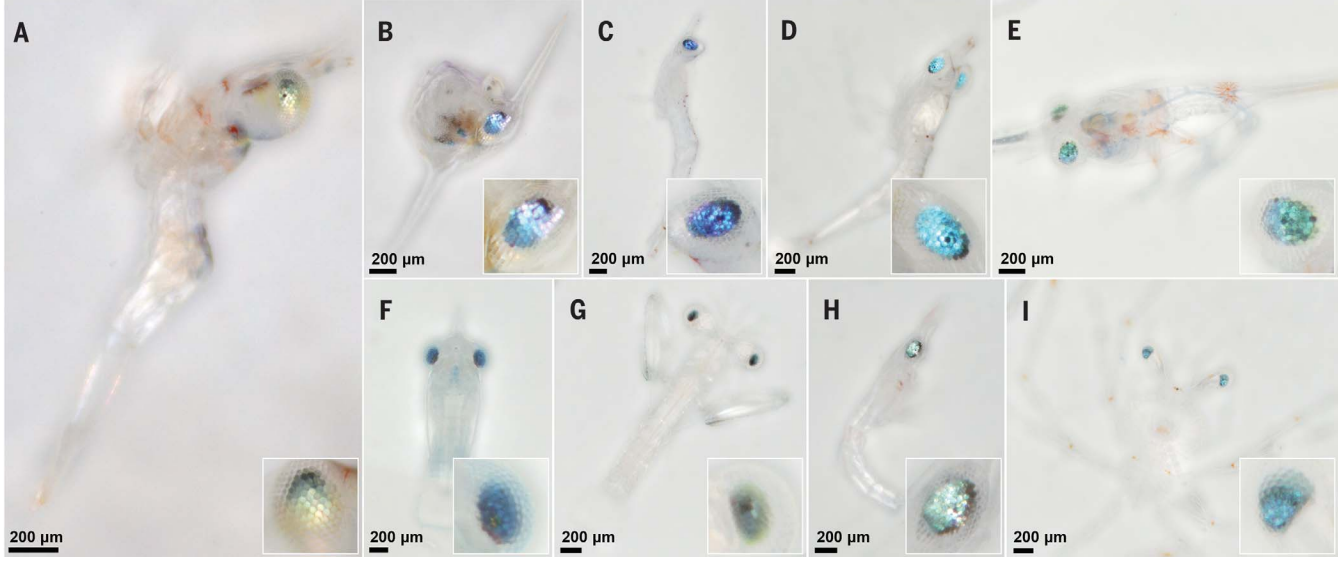

Fig. 1. Eyeshine reflectance in larval crustaceans. Polarized light micrographs of decapod and stomatopod larvae. (Insets) Higher-magnification images of the eyes. (**A**) A giant freshwater prawn, *M. rosenbergii* (development stage; zoea 2) (supplementary materials, materials and methods). (**B**) Zoea of a brachyuran crab. (**C** and **D**) Zoeae of caridean shrimp. (**E**) Zoea of a porcelain crab. (**F** and **G**) Stomatopod larvae. (**H**) Zoea of an axiid shrimp. (**I**) Phyllosoma of an achelate lobster.

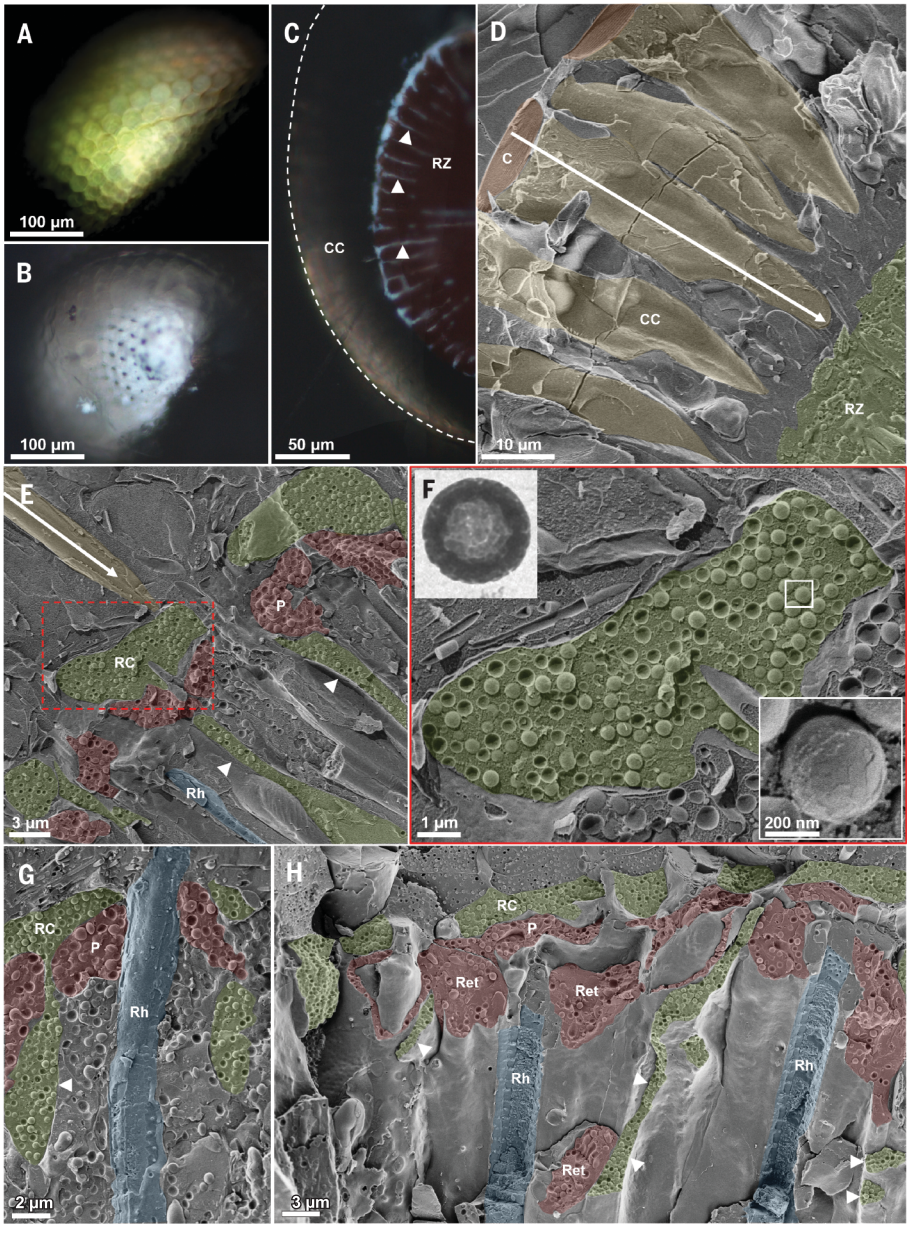

Fig. 2. Ultrastructure of the eyeshine reflector in *M. rosenbergii* larvae. (**A** to **C**) Polarizing optical micrographs of (A) a live eye (zoea 5), exhibiting yellow-green reflectance; (B) a cross section through a fixed eye (zoea 7); and (C) a longitudinal eye section viewed perpendicular to the eye's optic axis (zoea 7). Arrowheads indicate projections of the reflective cells extending into the retinal zone. Dashed trace denotes the boundary of the cornea. (**D** to **H**) Pseudo-colored cryo-SEM micrographs of longitudinal eye sections (zoea 4). (D) Low-magnification image of the eye showing the cornea (C; orange), crystalline cone (CC; yellow), and retinal zone (RZ; green). The arrow indicates the direction of the incident light. (E) Higher-magnification image showing the reflector cell (RC; green), screening pigment cells (P; red), and rhabdoms (Rh; blue). Projections of the reflective cells extend down the sides of the rhabdoms and retinal cells. (F) Region of interest in (E) showing a reflective cell comprising arrays of nanospheres. (Insets) (Top left) TEM and (bottom right) cryo-SEM micrographs of individual core-shell nanospheres that comprise concentric lamellae of isoxanthopterin crystal plates (*18*, *19*). The scale is the same in both insets. [(G) and (H)] As shown from two different angles, the reflector cells closely envelope the screening pigment, rhabdoms (Rh), and retinal cells (Ret). (G) is viewed perpendicular to the eyes optic axis, and (H) is at a more obtuse angle that shows the view along the ommatidia. In (H), the smooth, nonvesicular material surrounding the rhabdoms, pigment cells, and reflective cells are membranes. The labeling for the various eye structures in (C) to (H) was based on the anatomical descriptions provided in (*9*).

(cryo-SEM) (Fig. 2, D to H). Larval decapods have apposition eyes, constructed from hexagonal eye units called ommatidia (Fig. 2A) (*9*, *11*, *17*). The upper part of each ommatidium contains a proteinaceous body (the crystalline cone) that channels light onto the photoreceptors (Fig. 2, C to E). Polarizing optical micrographs viewed along the eye's optic axis reveal a highly reflective material at the base of the crystalline cones. The reflective material is absent from the optical pathway, allowing light from the cones to pass to the underlying photoreceptors (Fig. 2B). The reflective material also contains projections that extend into the retinal zone (Fig. 2C, arrowheads) that comprises the retinal cells, rhabdoms [the photoreceptive unit of crustacean eyes (*9*)], screening pigment cells, and nerve connections.

Cells (fig. S1) at the base of the cones contain assemblies of ~400-nm particles (Fig. 2, E and F). The particles are composed of crystalline isoxanthopterin (figs. S2 and S3) and are identical to those in the reflective tapetum of adult decapods (*18*, *19*). The extreme refractive index (n = 1.96) (*18*, *19*) nanospheres are constructed from a spherulitic assembly of single-crystal isoxanthopterin plates, arranged in lamellae around a hollow core (Fig. 2F, insets, and fig. S3). The anisotropic orientation of refractive indices arising from this spherulitic birefringence enhances scattering efficiency (*18*, *19*). Isoxanthopterin particles were present in all shrimp (fig. S4) and prawns we investigated, but a different reflective material is used in stomatopods or crabs (figs. S5 to S7). We attribute the eyeshine of *M. rosenbergii* and the marine shrimp to the isoxanthopterin-containing cells. The presence of isoxanthopterin in both the larval and adult shrimp reflectors suggests that the eyeshine reflector may be a developmental "precursor" to the adult tapetum (fig. S8) (*9*). Thus, a single material fulfills two distinct optical functions during development according to the changing visual ecology of the organism: the requirement for crypsis in larvae and dim light vision in adults (*17*).

On the dorsal side of the eye, the reflective cells form a reflective sheath around the absorbing pigment cells, effectively shielding them from view (Fig. 2, E, G, and H, and fig. S4). Conversely, the ventral side of the eye appears dark because the absorbing pigment lies on top of the reflective cells (fig. S9). Because larvae swim upside-down (*9*), the dorsal-lying reflective cells point downward, countershading the conspicuous eye pigments when viewed from below (*9*). The elongated projections of the reflective cells seen in optical micrographs (Fig. 2C) form a separation between adjacent rhabdoms (Fig. 2, E, G, and H) (*9*). The cellular extensions that interdigitate the rhabdoms are found in both the dorsal and ventral sides. This suggests that the reflective cells may serve a secondary function that directly enhances

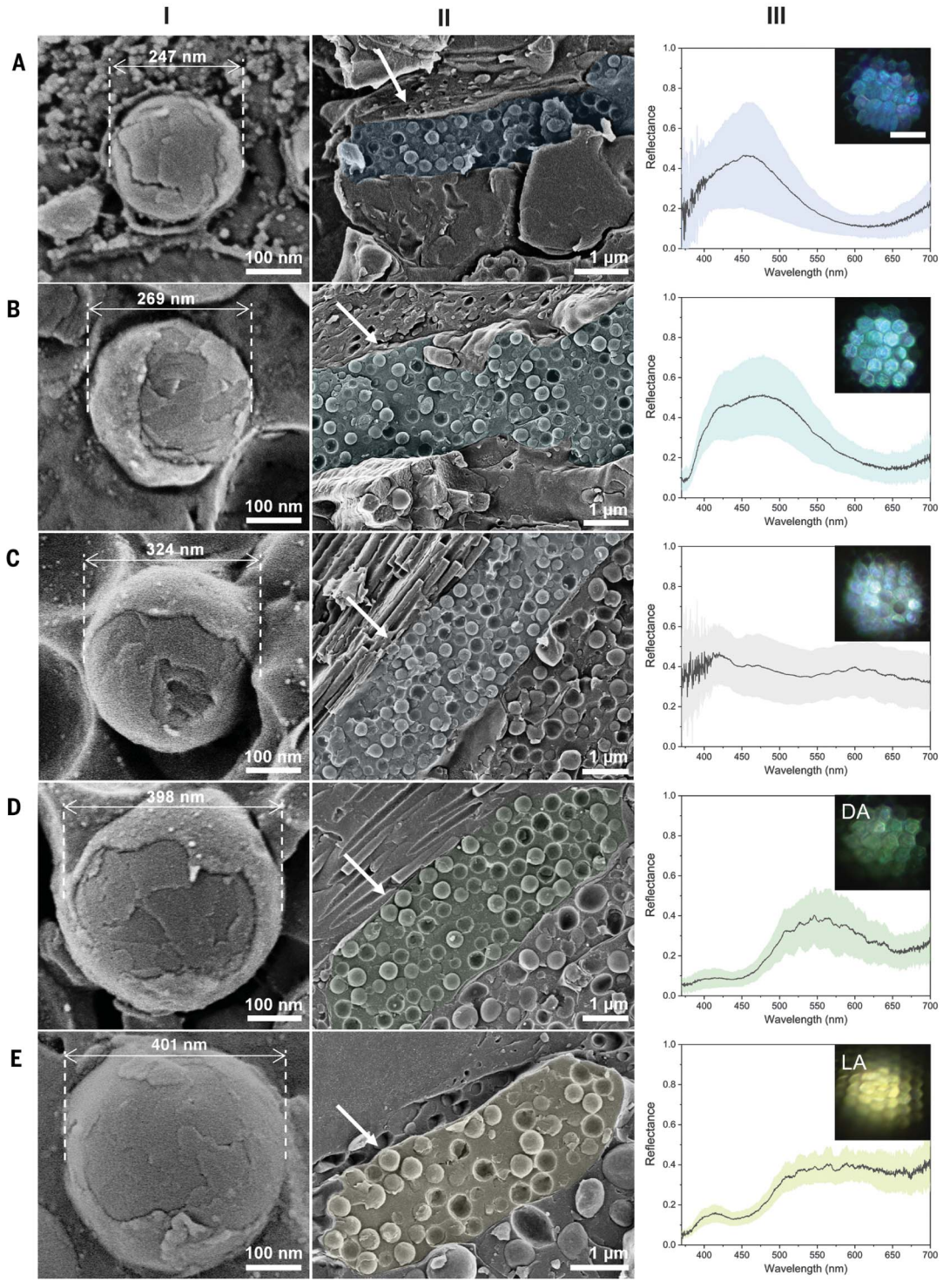

Fig. 3. The reflectance and structural properties of reflective cells in different shrimp and prawn larvae. Column I shows cryo-SEM images of single nanoparticles from a reflector cell. Column II shows representative cryo-SEM images of the reflector cells. White arrows indicate incident light direction. Column III shows the reflectance spectra from the eyes. Pastel shading indicates ±SD of the average reflectance across numerous specimens in the same color group (table S1). (Insets) Polarizing optical micrographs of the eyes. Scale bar, 50 µm and applies to all insets in column III. (**A** to **C**) Zoeae of different species of caridean shrimp from the Gulf of Aqaba. (**D**) Dark-adapted (DA) *M. rosenbergii* (zoea 6). (**E**) Light-adapted (LA) *M. rosenbergii*. Average particle sizes for the color groups are (A) blue, 247 nm (±7 nm, number of particles measured N = 398); (B) turquoise, 269 nm (± 15 nm, N = 400); (C) silvery blue, 324 nm (± 14 nm, N = 338); and (D) and (E) yellow-green (*M. rosenbergii*), DA, 398 nm (±30 nm, N = 179), and LA, 401 nm (±27 nm, N = 48). Average 2D filling fractions of the color groups are (A) blue, 57% (± 6%); (B) turquoise, 64% (± 5%); (C) silvery blue, 63% (± 7%); and (D) and (E) yellow-green (*M. rosenbergii*), DA, 63 ± 9%, and LA, 64 ± 5%.

vision—either as an additional screen between photoreceptors (*20*) to improve acuity or as a lateral tapetum-like structure that improves sensitivity during activity in dim light environments (*21*).

Correlation between the eyeshine color and nanosphere size

To rationalize the variation in eyeshine colors in the various shrimp and prawn species, we performed correlative cryo-SEM–reflectance measurements (Fig. 3). The eyeshine reflectance was measured and the shrimp grouped according to the position and shape of their reflectance peak(s). Four groups were assigned: (i) blue, exhibiting a narrow reflectance maximum around 450 nm (Fig. 3A); (ii) turquoise, exhibiting a broad reflectance band with maximum at 400 to 500 nm (Fig. 3B); (iii) silvery blue, exhibiting broadband reflectance with minor peaks at ~410 and ~600 nm (Fig. 3C); and (iv) yellow-green, exhibiting a broad reflectance maximum from 500 to 700 nm (*M. rosenbergii*) (Fig. 3, D and E). Cryo-SEM images of the reflective cells in the different groups revealed a clear correlation between the eyeshine color and the size of the component nanospheres. The reflectance shifted to longer wavelengths as the nanosphere diameter increased from ~250 nm in blue-eyed shrimp to ~400 nm in

the yellow-green *M. rosenbergii* (Fig. 3, A to E, and table S1).

Adaptation of the eyeshine reflector to camouflage in different habitats

These eyeshine colors appear to be well adapted to the background habitats of the different organisms. Larval marine shrimp exhibit blue to silvery blue eyeshine reflectance. The calculated eyeshine radiance of these organisms spectrally matches with the water radiance of the clear blue waters of the Gulf of Aqaba at different depths (Fig. 3, A to C, and figs. S10 to S15). Moreover, *M. rosenbergii*, *Macrobrachium amazonicum* (*10*), and *Palaemonetes pugio* (*9*), which inhabit estuaries [characterized by high organic content and turbid yellow water (*22*)], possess yellow-green eyeshine reflectance (Fig. 3, D and E, and fig. S16).

Feller and Cronin found (*3*) that the blue-green eyeshine of stomatopods was well matched to deeper depths in their marine environment and that depth was the key determinant in the visibility of the eyes. In our experiments, the marine shrimp shown in Fig. 3 were collected at night from shallow water (10 to 25 m), where they migrate from depth to feed (*23*). During the day, decapod larvae migrate to deeper depths to avoid predation from visual predators (*23*, *24*). In accordance with Feller and Cronin, our data suggest that the eyeshine of the marine shrimp can provide crypsis against the background of their daytime habitats at various depths (fig. S10 to S15).

Simulating the optical properties of the eyeshine reflector

To elucidate the optical mechanism underlying the eyeshine, we note that the upper limit (supplemenatry materials, materials and methods) of the two-dimensional (2D) particle filling fraction in the reflective cells was typically (Fig. 3 and fig. S4) between 50 and 70% (Fig. 3, column II), which is much lower than that of a close-packed photonic crystal (*25*). The nanospheres thus lack long-range periodicity but display the short-range positional ordering of a photonic glass structure. The scattering of photonic glasses is determined by an interplay between (i) the scattering properties of single particles (the form factor, F) and (ii) correlative scattering by particle ensembles (the structure factor, S) (Fig. 4A) (*26*). The absence of strong resonant peaks in form factor calculations indicates that single-particle scattering does not contribute appreciably to the optical response (Fig. 4, A and B). Conversely, strong structural peaks in the visible and infrared (IR) spectra in structure factor calculations may explain the experimental reflectance (Fig. 4C). We used molecular dynamics (MD) simulations to generate photonic glasses with particle sizes akin to those in the eyes and with a variety of filling fractions and structures (Fig. 4 and figs. S17 and S18). We simulated reflectance spectra using the finite-difference time domain (FDTD) technique (*18*, *27*) for each observed particle size (Fig. 4D and figs. S17 and S18). The simulated spectra reveal major peaks in the visible and IR (Fig. 4D), corresponding to the second- and first-order structural peaks predicted with numerical calculations, respectively

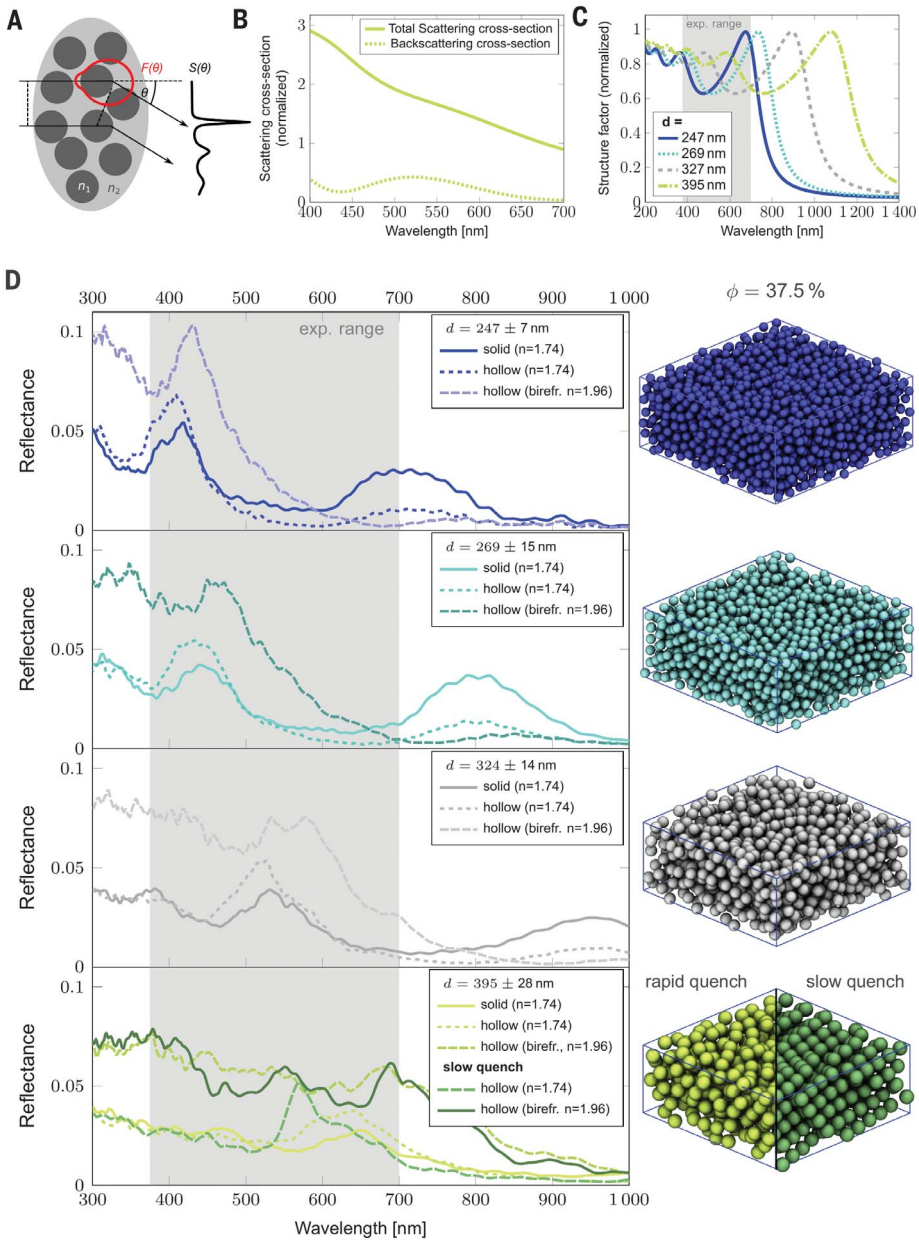

Fig. 4. Optical modeling of the eyeshine phenomena. (**A**) A schematic of the form $F(\theta)$ and structure factor $S(\theta)$ contributions to the scattering of a photonic glass. (**B**) Total (solid trace) and backscattering (dotted trace) cross sections for a spherical particle found in *M. rosenbergii* (diameter, 395 nm; refractive indices of particle and medium, respectively, $n_{particle} = 1.96$, $n_{medium} = 1.33$) calculated with Mie theory (*34*). No resonance peak in the visible spectrum is observed in the total scattering in contrast to the experimental reflectance (Fig. 3). The backscattering spectra exhibits a low-intensity peak in the visible spectrum, which is much broader than in the experimental spectra. (**C**) Percus-Yevick structure factor (*35*) for the experimentally observed particle sizes with a 3D filling fraction of 50%, by using the Garnett effective refractive index for the system (*36*). The first-order structural peak is in the red and IR, whereas a second-order peak lies in the visible spectrum. (**D**) MD and FDTD simulations of 2- by 5- by 5-μm photonic glass slabs by using a lower-bound estimate (37.5%) of the 3D filling fraction. (Left) Simulated spectra of solid (n = 1.74), hollow (n = 1.74), and hollow-birefringent particles (n = 1.96) for the four experimentally observed particle sizes. (Right) Snapshot of the MD-simulated particle configurations. For the 395-nm particle, a composite image is shown for rapid (disordered; yellow) and slow quench (more crystalline; green) states, simulating the dark-light adaption observed in *M. rosenbergii*.

(Fig. 4C). The position of the visible peak correlates with the experimental reflectance and red-shifts with increasing particle size (Fig. 4D and fig. S19). Simulations using hollow and hollow-birefringent spheres led to an enhancement in the intensity of the visible peak and a suppression of the IR peak compared with those of solid isotropic particles. Although the IR reflectance is unlikely to be biologically relevant, particle hollowness and birefringence are seemingly used as a means of enhancing scattering efficiency in the visible spectrum. The increased intensity of the birefringent nanospheres is likely due to their higher refractive index (n = 1.96), resulting from the anisotropic alignment of the component refractive indices in the spheres (*18*). The reflectance intensities obtained from simulations are lower than the experimental spectra (Fig. 3) because of the small size of the computed photonic glasses (fig. S20) and experimental factors (such as specular reflection).

Further evidence for the role of structural correlations in the optical response came from the observation that the eyeshine of *M. rosenbergii* changes reversibly in different light conditions. Dark-adapted (DA) larvae have green eyeshine, with a large reflectance peak at ~560 nm (Fig. 3D). Upon light adaptation, the peak broadens, resulting in silvery yellow eyeshine (Fig. 3E). This dynamically changing eyeshine indicates that *M. rosenbergii* may spectrally match its eyeshine appearance to a temporally changing background, which may be relevant during diel vertical migrations (fig. S16) (*23*). Cryo-SEM imaging shows that the particle size, filling fraction, and absorbing pigment distribution in DA and light-adapted (LA) eyes are constant (fig. S21 and table S1). However, upon dark adaptation, spatial correlations in the particle arrangement emerge, which is manifest in the presence of disordered multilayers consisting of three to five layers of particles (Fig. 3D and fig. S21).

To rationalize the light-dark adaptation behavior, MD simulations were performed in which the 395-nm particles were allowed to equilibrate during a slow quench to achieve a more well-ordered particle packing (Fig. 4D and fig. S22). In comparison with the normal glassy state, simulations that used hollow and hollow-birefringent spheres in this configuration led to an emergence of a reflectance peak around 550 to 600 nm, resembling the changes in DA and LA *M. rosenbergii* (Fig. 3, D and E). The position of this peak aligns with that of an ordered face-centered cubic lattice of such particles, suggesting the structural origin of this reflectance peak. In general, the simulated spectra exhibit narrower peaks than the experimental ones because the latter represent the convoluted optical response from multiple cells encompassed in the illumination volume (an average over variations in filling fraction, sample thickness, degree of disorder, and particle polydispersity).

Discussion

Our results show that decapod eyeshine reflectance is generated by a photonic glass constructed from crystalline isoxanthopterin nanospheres, whose location overlying the screening pigments is consistent with a camouflage function (*3*). Reflectors are widely used in animal eyes, and their function depends on their location, nanostructure, and composition (*28*). Concave and radial mirrors form images in scallop (*29*) and decapod crustacean eyes (*17*, *19*), respectively, and in many organisms, tapetal reflectors enhance sensitivity by back-scattering light to the photoreceptors (*17*). Mirrored irises in fish prevent unfocused light entering the eye to preserve visual acuity (*7*). Reflectors in the cornea of insects (*30*) or embedded within the photoreceptors of crustaceans (*21*) spectrally filter light impinging on the retinas. Ocular reflectors can also perform nonvisual functions. For example, basally located *stratum argenteum* reflectors in fish eyes enhance camouflage by reducing the visibility of the pupil (*31*).

A distinguishing feature of the eyeshine reflector described here is its tunability and compactness. Across different larval shrimp and prawn species, the eyeshine color is modulated by tuning the size of the isoxanthopterin nanospheres in the photonic glass. Within a single species, eyeshine color can be changed by tuning the particle ordering. Feller and Cronin predicted (*3*) that because larval crustacean eyes are minute, the underlying photonic structure must be ultracompact and efficient, unlike the disordered multilayer reflectors of fish scales (*32*), which occupy space unavailable in the larval eyes. However, the most efficient photonic structures—ordered quarter-wave stacks and photonic crystals (*25*)—produce iridescence (*25*), meaning that the color would vary with viewing angle, which is not usually (*33*) advantageous for crypsis. The use of a photonic glass, comprising high-index isoxanthopterin particles, enables efficient, angle-independent colors to be produced, simultaneously fulfilling the demands of crypsis (from all angles) and compactness. There is a strong selective pressure for transparent prey animals to reduce the size and visibility of their eyes (*5*, *6*). However, small eyes have lower resolution, and thus there is an intrinsic trade-off between the visibility of the eyes and the ability to see (*3*). The presence of reflective cell projections between the rhabdoms suggests that the eyeshine reflector may also function to screen adjacent photoreceptors (*20*). The enhanced screening efficiency provided by a reflective material (compared with an absorbing screening pigment) may enable the rhabdoms to be more tightly packed, mitigating against the cost to visual acuity of having minute eyes. Our studies elucidate design strategies for tuning the properties of biocompatible optical materials: by controlling the size, ordering, hollowness, and birefringence of the component particles.

REFERENCES AND NOTES

1. S. Johnsen, *Biol. Bull.* **201**, 301–318 (2001).
2. T. W. Cronin, M. J. Bok, C. Lin, *Integr. Comp. Biol.* **57**, 1139–1150 (2017).
3. K. D. Feller, T. W. Cronin, *J. Exp. Biol.* **217**, 3263–3273 (2014).
4. S. Johnsen, *Ann. Rev. Mar. Sci.* **6**, 369–392 (2014).
5. R. Svanbäck, F. Johansson, *Proc. Biol. Sci.* **286**, 20182625 (2019).
6. D. E. Nilsson, *Nature* **302**, 818–821 (1983).
7. D. Gur *et al*., *Adv. Sci.* **5**, 1800338 (2018).
8. S. Harzsch, J. Benton, R. R. Dawirs, B. Beltz, *J. Neurobiol.* **39**, 294–306 (1999).
9. J. K. Douglass, R. B. Forward Jr., *Cell Tissue Res.* **258**, 289–300 (1989).
10. K. Anger, L. Hayd, *Aquat. Biol.* **7**, 19–30 (2009).
11. T. W. Cronin, R. N. Jinks, *Am. Zool.* **41**, 1098–1107 (2001).
12. L. Schertel *et al*., *Adv. Opt. Mater.* **7**, 1900442 (2019).
13. S. Magkiriadou, J. G. Park, Y. S. Kim, V. N. Manoharan, *Phys. Rev. E Stat. Nonlin. Soft Matter Phys.* **90**, 062302 (2014).
14. G. Jacucci, S. Vignolini, L. Schertel, *Proc. Natl. Acad. Sci. U.S.A.* **117**, 23345–23349 (2020).
15. M. J. Henze, O. Lind, B. D. Wilts, A. Kelber, *J. R. Soc. Interface* **16**, 20180785 (2019).
16. H. Noh *et al*., *Adv. Mater.* **22**, 2871–2880 (2010).
17. M. F. Land, D. E. Nilsson, *Animal Eyes* (Oxford Univ. Press, ed. 2, 2012).
18. B. A. Palmer *et al*., *Nat. Nanotechnol.* **15**, 138–144 (2020).
19. B. A. Palmer *et al*., *Proc. Natl. Acad. Sci. U.S.A.* **115**, 2299–2304 (2018).
20. E. Hallberg, R. Elofsson, *J. Crustac. Biol.* **9**, 359–372 (1989).
21. K. D. Feller *et al*., *Curr. Biol.* **29**, 3101–3108.e4 (2019).
22. D. G. Bowers, D. Evans, D. N. Thomas, K. Ellis, P. J. B. Williams, *Estuar. Coast. Shelf Sci.* **59**, 13–20 (2004).
23. R. B. Jr., *Oceanogr. Mar. Biol. Annu. Rev.* **26**, 1–393 (1988).
24. J. Marshall, J. Kent, T. Cronin, in *Adaptive Mechanisms in the Ecology of Vision*, S. N. Archer, M. B. A. Djamgoz, E. R. Loew, J. C. Partridge, S. Vallerga, Eds. (Springer, 1999), pp. 285–327.
25. S. Kinoshita, S. Yoshioka, J. Miyazaki, *Rep. Prog. Phys.* **71**, 076401 (2008).
26. S. Fraden, G. Maret, *Phys. Rev. Lett.* **65**, 512–515 (1990).
27. B. D. Wilts, K. Michielsen, H. De Raedt, D. G. Stavenga, *Proc. Natl. Acad. Sci. U.S.A.* **111**, 4363–4368 (2014).
28. B. A. Palmer, D. Gur, S. Weiner, L. Addadi, D. Oron, *Adv. Mater.* **30**, e1800006 (2018).
29. B. A. Palmer *et al*., *Science* **358**, 1172–1175 (2017).
30. D. G. Stavenga *et al*., *J. Comp. Physiol. A Neuroethol. Sens. Neural Behav. Physiol.* **203**, 23–33 (2017).
31. M. Santon, P.-P. Bitton, U. K. Harant, N. K. Michiels, *Sci. Rep.* **8**, 7368 (2018).
32. T. M. Jordan, J. C. Partridge, N. W. Roberts, *Nat. Photonics* **6**, 759–763 (2012).
33. K. Kjernsmo *et al*., *Curr. Biol.* **30**, 551–555.e3 (2020).
34. C. F. Bohren, D. R. Huffman, *Absorption and Scattering of Light by Small Particles* (Wiley, 2008).
35. J. K. Percus, G. J. Yevick, *Phys. Rev.* **110**, 1–13 (1958).
36. J. C. M. Garnett, *Philos. Trans. Royal Soc. A* **203**, 385–420 (1904).
37. K. Shavit *et al*., Data and code for: "A tunable reflector enabling crustaceans to see but not be seen". Zenodo (2023); https://doi.org/10.5281/zenodo.7566611.

ACKNOWLEDGMENTS

We acknowledge M. Pavan for assistance with Raman spectroscopy; T. Levy, Y. Molcho, and R. Manor for valuable discussions on the manuscript; and E. Sestieri for help in shrimp collection. **Funding:** This work was supported by ERC Starting Grant (grant 852948, "CRYSTALEYES") awarded to B.A.P.; B.A.P. is the Nahum Guzik Presidential Recruit and a recipient of the 2019 Azrieli Faculty Fellowship. This work was also supported by the European Union's Horizon 2020 research and innovation program under the Marie Skłodowska-Curie grant agreement (893136) awarded to J.H. and a Swiss National Science Foundation Grant (grant 40B1-0_198708) awarded to L.S. Electron microscopy studies were supported by the Ilse Katz Institute for Nanoscale Science & Technology at Ben-Gurion University of the

Negev. **Author contributions:** Conceptualization: K.S., V.J.Y., and B.A.P. Methodology: K.S., L.S., V.J.Y., J.H., and B.A.P. Investigation: K.S., A.W., L.S., V.F., D.A., G.Z., A.U., J.H., and B.A.P. Funding acquisition: B.A.P. Supervision: A.S. and B.A.P. Writing – original draft: K.S., L.S., J.H., and B.A.P. Writing – review and editing: K.S., A.W., L.S., V.F., D.A., J.H., and B.A.P. **Competing interests:** The authors declare that they have no competing interests. **Data and materials availability:** All data are available in the main text or the supplementary materials. Raw data and relevant code can be found at (*37*).

SUPPLEMENTARY MATERIALS

science.org/doi/10.1126/science.add4099
Materials and Methods
Figs. S1 to S22
Table S1
References (*38*–*50*)
MDAR Reproducibility Checklist

View/request a protocol for this paper from *Bio-protocol*.

Submitted 9 June 2022; accepted 24 November 2022
10.1126/science.add4099

A tunable reflector enabling crustaceans to see but not be seen

Keshet Shavit, Avital Wagner, Lukas Schertel, Viviana Farstey, Derya Akkaynak, Gan Zhang, Alexander Upcher, Amir Sagi, Venkata Jayasurya Yallapragada, Johannes Haataja, and Benjamin A. Palmer

Science, **379** (6633), .
DOI: 10.1126/science.add4099

A photonic glass to camouflage crustaceans

Eye pigments are usually required for vision, but for creatures that want to stay hidden, they make it easier to be seen by others. This raises the question how marine invertebrates avoid being detected. Studying larval crustaceans, Shavit *et al*. found that many of these animals use an ultracompact reflector that overlies the opaque eye pigments and conceals them from view (see the Perspective by Feller and Porter). The reflection of light from the inner surface of the eye is produced by a photonic glass comprising crystalline isoxanthopterin nanospheres. The size and ordering of the nanospheres is varied to tune the reflectance from deep blue to yellow-green, enabling the organisms to blend in with different habitats. The use of a photonic glass may also enhance the vision of the eye. —MSL